

Article

Primary Phases and Natural Weathering of Smelting Slag at an Abandoned Mine Site in Southwest Japan

Yuri Sueoka * and Masayuki Sakakibara

Graduated School of Science and Engineering, Ehime University, Bunkyo-cho 2-5, Matsuyama, Ehime 790-8577, Japan; E-Mail: sakakiba@sci.ehime-u.ac.jp

* Author to whom correspondence should be addressed; E-Mail: sueoka@sci.ehime-u.ac.jp; Tel.: +81-089-927-9649; Fax: +81-089-927-9640.

Received: 12 October 2013; in revised form: 26 November 2013 / Accepted: 28 November 2013 / Published: 13 December 2013

Abstract: Artisanal metallurgical slag produced more than 50 years ago at a mine site in southwest Japan is rich in toxic metals and metalloids. Some of the slag remains on a waste dump and could contaminate the surrounding area through the dissolution of heavy metals and metalloids during weathering. To assess this risk, this study has investigated the behavior of the toxic elements in the smelting slag during weathering. Most of the potentially toxic elements are contained in willemite and/or matte drops. Maximum metal and metalloid concentrations in the slag are 28.1 wt % Fe, 22.7 wt % Zn, 1.63 wt % Cu, 3450 mg/kg Sn, 826 mg/kg Pb, 780 mg/kg As, and 116 mg/kg Cd. Zn is mainly contained in willemite, whereas other metals and metalloids are mainly concentrated in matte drops. The willemite and matte drops are converted to Fe-hydroxides during weathering, indicating that potentially toxic metals and metalloids contained in these phases are released by weathering processes. Therefore, weathering of the artisanal metallurgical slag, containing large amounts of willemite and matte drops, may pollute the surrounding environment.

Keywords: slag; weathering; Zn; Cu; pollution; willemite; matte drop

1. Introduction

Slag is a waste material produced by smelting processes. Melting of ore concentrate sequesters elements into gas, slag, or matte phases depending on the chemical and physical characteristics of each element. The waste slag produced by small-scale, artisanal metallurgical smelting processes contains

high concentrations of toxic elements, as it contains large amounts of material of matte origin, which occur as matte drops [1–3]. Some of this artisanal metallurgical slag remains on-site in waste dumps throughout Japan, and is exposed to rain and wind. The present study site is under similar conditions. Exposure and weathering of slag, leading to the dissolution of potentially toxic elements, could cause toxic metal and metalloid contamination of the surrounding environment including soil, ground water, and surface water [4–8].

The nature of secondary phases in slag dumps has been reported in previous studies [9–11]. The presence of secondary phases reflects reactions between the slag and water/atmosphere. The secondary phases are produced during weathering, caused by rain and changes in the pH of percolating water [12]. During this weathering, potentially harmful elements may be released from the primary and secondary slag phases. Laboratory leachate experiments also suggest that considerable amounts of Cu, Zn, As, Sb, and Pb are released from slag during weathering, and the concentrations of some elements exceed the United States Environmental Protection Agency chronic toxicity guidelines for aquatic habitats by several orders of magnitude [13].

Slag containing high proportions of glass is more hazardous than low-glass slag because heavy metals in crystalline silicates and oxides are not significantly mobilized by short-term weathering under neutral pH conditions [14,15]. However, metals can be released from primary silicate, oxide, sulfide and carbonate phases over a wide range of pH conditions during short and long-term weathering [16–19].

The present study area is a small-scale mine site and waste dump where the artisanal metallurgical slags are still on-site. Slag exposure to rain and wind is enhanced due to sparse vegetation, with the exception of the fern *Athyrium yokoscense*, which is known to be a bioindicator of Cu, Zn, and Cd [20]. The pH of the stream water in the dumpsite is nearly neutral (pH of 7.2–7.8). The water contains 1910 wt % Zn and 43.1 wt % As, and these concentrations are in excess of environmental water quality standards stipulated by the Ministry of Health, Labor, and Welfare in Japan [21]. The stream sediment also contains 4630 mg/kg-DW* As and 286 mg/kg-DW* Pb, and these levels exceed Japan's environmental quality standards stipulated by the Ministry of the Environment (DW*: dry weight) [21]. One of the potential contaminant origins is the Zn-rich, artisanal metallurgical slag on the dumpsite, which contains potentially toxic metals and metalloids.

Some artisanal metallurgical slag at the present study site that cooled under atmospheric conditions contains a higher proportion of Fe- and/or Zn-rich crystalline phases. In addition, the primary phases contain higher concentrations of potentially harmful metals and metalloids than present in glass. However, the dissolution of potentially toxic elements from crystalline phases under natural conditions has not been studied in detail, due to the stability of crystalline phases as compared with glass under neutral pH conditions. Clarification of the material balance of pollutants is important when evaluating pollution in a given area. Therefore, in this study we have investigated the behavior of potentially toxic metals and metalloids in primary silicate, sulfides, and metallic phases in smelting slag, which is a potential source of pollution, during weathering of the slag at the dumpsite.

2. Materials and Methods

2.1. Study Area and Materials

The study area is located at an abandoned unnamed mine site in western Okayama, southwest Japan at an altitude of approximately 250 m above sea level, located in the temperate zone with an average temperature of 14.1 °C (seasonal averages: 2.5 °C in February and 27.7 °C in August) and a total annual precipitation in 2012 of 1257 mm (seasonal totals: 23.0 mm in January and 285 mm in July) (Figure 1). The area was the site of smelting of Au, Ag, Cu, Pb, Zn, and As. There are no detailed records of the mining operation, due to the small-scale and artisanal nature of the metallurgical mining. Host rocks around the mine site are rhyolite, andesite, sandstone, mudstone, and phreatomagmatic breccias, and include pyrite and chalcopyrite with quartz and calcite veins. The composition of the tailing dump indicates that the ore smelted in this area was mainly phreatomagmatic breccias and rhyolite. The surface of the mine tailing dump mainly comprises fractured slag that overlies solidified, coherent slag (Figure 2b,c). The fractured waste slag has in part been kept on-site by wooden boards, although these are now decaying and no longer effective.

Figure 1. A location map of study area (indicated by black dots).

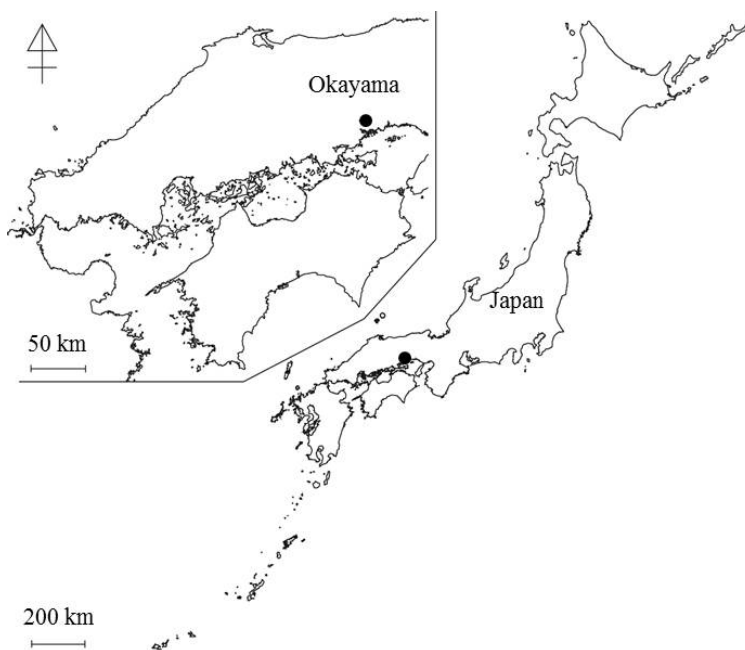
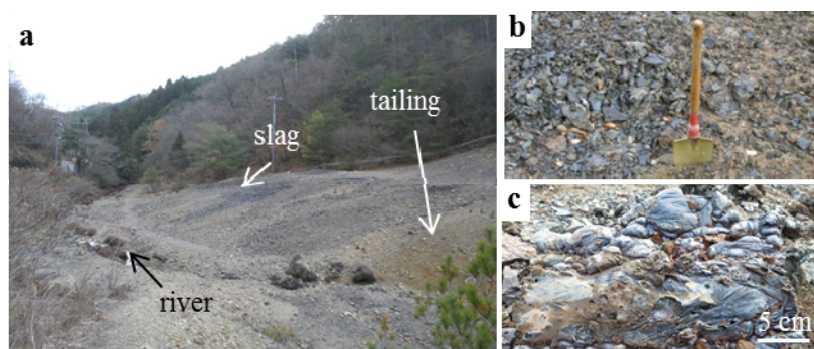


Figure 2. Photographs of (a) waste dumpsite, (b) fractured slag, and (c) coherent slag on the dumpsite.



2.2. Analytical Methods

Primary and subsidiary phases in the slag were investigated by X-ray powder diffraction analysis (XRD) and a scanning electron microscope equipped with an energy dispersive X-ray spectrometer (SEM-EDS), for identification of the phases. Thirty fractured slags and five coherent slags were sampled at random from the mine dump and observed with polarized-light microscopy and/or SEM. A subset of nine fractured slags and three coherent slags was analyzed by SEM-EDS to investigate the distribution of potentially toxic elements in the slag. The vesicle-rich and major-massive components, and the matte drop-rich component within the massive portion, were analyzed in the individual coherent slags. Five fractured slags and each component of three coherent slags were also analyzed by XRD. These eight samples (three samples in willemite-rich assemblage I, four samples in fayalite-rich assemblage II, and one sample in magnetite-rich assemblage III) were also analyzed by energy dispersive X-ray fluorescence (ED-XRF) to determine the metal and metalloid concentrations in the slag.

Eight pulverized samples were analyzed by XRD to identify the mineral components in the slag. XRD analyses were performed on a Ultima IV (Rigaku, Tokyo, Japan) spectrometer housed at Ehime University (Japan) using $\text{CuK}\alpha$ ($\lambda = 1.54056 \text{ \AA}$) radiation. The diffraction patterns for non-constant azimuth analysis were collected using an accelerating voltage of 40 kV, specimen current of 40 mA, with an analytical speed of $2^\circ/\text{min}$, and analytical range of $5^\circ\text{--}70^\circ$.

Twelve slag samples were imaged and analyzed by SEM-EDS on a JSM-6510LV (JEOL, Tokyo, Japan) (SEM) and X-Max 50 (Oxford Instruments, Tokyo, Japan) detector with INCA software (Oxford Instruments) at Ehime University. The slag samples were embedded in resin and prepared as polished thin sections, which were then carbon-coated. The glass-phase content in the slag was estimated by counting at the intersection points of 200 μm mesh overlaid on back-scattered electron images. The SEM was operated with an accelerating voltage of 15 kV and beam current of 0.8 nA. A counting time of 50 s was used for quantitative analysis, and count times of >1 h were required for element mapping. Enstatite (MgSiO_3), K-feldspar (KAlSi_3O_8), and anorthite ($\text{CaAl}_2\text{Si}_2\text{O}_8$) (Japan Electron Optics Laboratory Mineral Standard Samples for Electron Probe Micro Analyzer) were analyzed to confirm the analytical precision and accuracy. The following standards were used: $\text{NaAlSi}_2\text{O}_6$ for Na, Mg_2SiO_4 for Mg, Al_2O_3 for Al, CaSiO_3 for Si, FeS_2 for S, KBr for K, Ti for Ti, Cr for Cr, Mn for Mn, FeS_2 for Fe of matte drops, Fe_2O_3 for Fe of magnetite, Fe_2SiO_4 for Fe of fayalite and glass, Co for Co, Cu for Cu, ZnO-glass for Zn, InAs for As, Ag for Ag, and Sn for Sn. Co standard was also used to optimize the quantification of the analyses. The L characteristic X-ray lines were used for Cu, Zn, As, Ag, and Sn quantification; the K lines were used for other elements. The quantitative values were selected according to Curie's detection limit (3.29σ).

Metal and metalloid concentrations of the slag were determined by ED-XRF spectrometry using an Epsilon5 instrument (PANalytical, Almelo, The Netherlands) at Ehime University. Pressed powder pellet samples were used for the XRF analysis. Samples were powdered to a grain size of $<1 \mu\text{m}$ in a tungsten carbide vibrating sample mill (SAMPLE MILL model TI-100) (HEIKO, Tokyo, Japan) at Ehime University and an agate mortar. $\text{C}_{13}\text{H}_{14}\text{O}_6$ was used as a binder (25 wt % in the pressed powder pellets) and was homogenized with powdered samples by shaking for 1 h. The XRF analyses were conducted at an excitation voltage of 100 kV. The following standards were used as

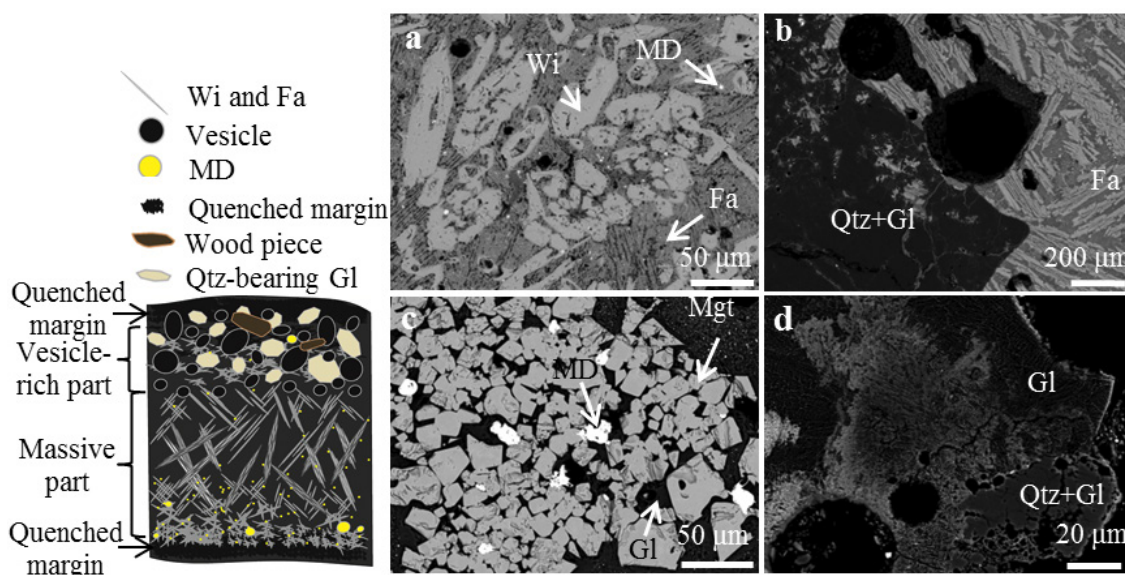
secondary targets for irradiation with relevant excited X-rays for individual elements: Al for Na and Mg; Ti for Al-Sc; Ge for Ti-Ga; Mo for Ge-Y, Tl-Ra, and Ac-U; and Al_2O_3 for other elements including lanthanoids. The X-ray source was a Gd anode. A counting time of 300 s was repeated three times on a Ge detector for each secondary target, and elemental concentrations were determined by the fundamental parameter method. Geological standards, including JSd-1, JSd-2, JSd-3, JSI-1, Jlk-1, and JMn-1 (Geological Survey of Japan Referenced Materials) [22,23], were analyzed to confirm the analytical precision and accuracy (Relative standard deviations are 1.86% Fe_2O_3 ; 11.3% Cu; 3.09% Zn; 10.9% As; 45.5% Sn; 53.2% Pb).

3. Results and Discussion

3.1. Phases Observations

The coherent slag has three parts, based on the dominant phases present (Figure 3). The vesicle-rich component of the slag contains a larger proportion of vesicles, glassy material, and pieces of wood compared with the rest of the slag. The massive component of the slag is dominated by willemite, fayalite, and/or magnetite. The proportion of matte drops in the massive component gradually increases toward the edge of the coherent slag pile, but matte drops are absent in the quenched margin of the pile. This gradation indicates that the matte drops settle out by gravity until the slag is solidified.

Figure 3. A schematic cross-section of a massive slag and back-scattered electron images of (a) assemblage I in massive component, (b) assemblage II in vesicle-rich component, (c) assemblage III in massive component, and (d) quenched margin of the slag. Qtz: quartz; Fa: fayalite; Wi: willemite; Mgt: magnetite; Gl: glass; MD: matte drop.



The grain size of the crystalline phases depends on the cooling rate, which in turn depends on the distance from the surface of the coherent slag. The quenched outer part of the slag is mainly composed of glass and sporadic micro-crystals. Crystals in the surface zone have a variolitic structure similar to that in basalt. Willemite and/or fayalite in the deeper part of the coherent slag exhibit a spinifex texture

similar to that in komatiites. The glassy matrix contains dendritic and skeletal fayalite, and fine-grained (<1–3 μm) matte drops.

3.2. Primary Slag phases

3.2.1. Slag Classification According to Primary Phases

The slag is composed of Zn–Fe silicates (willemite and fayalite), magnetite, sulfides, alloys, metallic phases, glass, spinel, quartz, and feldspar (Table 1). The quartz and feldspar are sometimes contained within the silicate glass phase. Most of the slag, especially in the massive portion, is heterogeneous. The variable mineralogical assemblages are as follows (in order of formation): (1) Assemblage I: willemite–fayalite–matte drops–silicate glass; (2) Assemblage II: fayalite–(magnetite)–matte drops–silicate glass; and (3) Assemblage III: magnetite–matte drops–silicate glass.

Table 1. Primary phases and subsidiary phases of the slag obtained by X-ray powder diffraction analysis (XRD) and energy dispersive spectrometer (EDS) (normal: both methods; italics: only EDS).

Group	Name	Composition	Assemblage I	Assemblage II	Assemblage III
Silicates	Willemite	Zn ₂ SiO ₄	***		
	Fayalite	Fe ₂ SiO ₄	**	***	
	Albite	NaAlSi ₃ O ₈	*	*	*
	Anorthite	CaAl ₂ Si ₂ O ₈	*	*	*
	Quartz	SiO ₂	*	*	*
	<i>Glass</i>	<i>Al-Si-Fe-Zn-O</i>	*	*	**
Oxides	Magnetite	Fe ²⁺ Fe ³⁺ ₂ O ₄		*	***
	<i>Gahnite</i>	<i>ZnAl₂O₄</i>	*	*	
Sulfides	Sphalerite	ZnS	*	*	
	<i>Chalcocite</i>	<i>Cu₂S</i>	*	*	*
	<i>Bornite</i>	<i>Cu₅FeS₄</i>	*	*	
	<i>Geerite</i>	<i>Cu₈S₅</i>	*	*	
Element	<i>Cu</i>		*	*	*
Others	<i>Alloys</i>	<i>Cu-Fe</i>	*	*	*
	<i>Suphides and Arsenides</i>	<i>Cu-Sn-Fe-S</i>	*	*	
		<i>Cu-Fe-Zn(±S±As)</i>	*	*	

Notes: ***: major (>60%); **: minor (<30%); *: trace (<10%).

Assemblage I is mainly composed of euhedral or subhedral willemite, set in a matrix of dendritic fayalite and silicate glass. The glass contains micro-skeletal fayalite and micro-particles of matte drops (<1–3 μm). Assemblage II consists mainly of dendritic fayalite. Euhedral and/or subhedral magnetite is occasionally present. The matrix is composed of dendritic/skeletal fayalite and silicate glass. The glass contains micro-skeletal fayalite and micro-particles of matte drops (<1–3 μm). Assemblage III is mainly composed of euhedral and skeletal magnetite set in a matrix of silicate glass. The glass contains micro-particles of matte drops (<1–3 μm). Assemblage I is dominant in the slag, whereas assemblage III is relatively rare. All assemblages contain metals, alloys, sulfides, and arsenides as matte drops, and

contain anhedral quartz and feldspar within glass. The quartz and feldspars were identified by XRD analysis, but are not readily identified optically by polarized-light microscopy.

3.2.2. Olivine and Spinel Group Phases

Willemite (Zn_2SiO_4) is a trigonal mineral of the phenakite group. The willemite in assemblage I is typically Fe-rich and contains up to 19.89 wt % FeO, but is Mg-poor (Table 2). In comparison, willemite from base-metal slag produced by historical Cu smelting at Penn Mine in California contains on average 0.76 wt % FeO and 2.32 wt % MgO [24]. The Fe atomic proportion in assemblage I is approximately $\text{Fe}/(\text{Zn} + \text{Fe} + \text{Mg}) = 0.28\text{--}0.42$, with an empirical formula of $(\text{Zn}_{1.24}\text{Fe}_{0.73}\text{Mg}_{0.03})\text{SiO}_4$.

Fayalite (Fe_2SiO_4) is an orthorhombic mineral of the olivine group. The fayalite in assemblage I is typically Zn-rich and contains up to 13.74 wt % ZnO, but is also Mg-poor (Table 2). In contrast, fayalite from base-metal slag produced by historical Cu smelting at Penn Mine in California contains on average 6.83 wt % ZnO and 8.63 wt % MgO [24]. The Zn atomic proportion in assemblage I is approximately $\text{Zn}/(\text{Zn} + \text{Fe} + \text{Mg}) = 0.16\text{--}0.24$, whereas in the other assemblage it is approximately $\text{Zn}/(\text{Zn} + \text{Fe} + \text{Mg}) = 0.08\text{--}0.10$. The empirical formula of fayalite in assemblage I is $(\text{Fe}_{1.62}\text{Zn}_{0.35}\text{Mg}_{0.03})\text{SiO}_4$.

Table 2. Chemical compositions of willemite and fayalite obtained by EDS. Structural formulae (apfu: atoms per formula unit) were calculated on the basis of four oxygens.

Phases	Willemite		Fayalite					
	Assemblage I		Assemblage I		Assemblage II		Assemblage III	
SiO ₂ (wt %)	27.76	27.56	28.33	28.46	28.79	28.77	31.13	34.58
FeO (wt %)	19.62	19.89	57.67	56.47	63.84	62.74	62.29	57.96
MgO (wt %)	0.77	0.62	0.77	0.54	1.14	0.95	0.91	0.93
ZnO (wt %)	52.68	51.64	13.44	13.74	6.25	7.30	6.83	6.06
Total (wt %)	100.83	99.71	100.21	99.21	100.02	99.76	101.16	99.53
Si (apfu)	0.99	1.00	0.97	0.99	0.98	0.98	1.03	1.12
Fe ²⁺ (apfu)	0.59	0.60	1.68	1.65	1.83	1.80	1.73	1.57
Mg (apfu)	0.04	0.03	0.04	0.03	0.06	0.05	0.04	0.04
Zn (apfu)	1.39	1.34	0.34	0.35	0.16	0.18	0.17	0.14

The range of Zn/Fe ratios of the willemite and fayalite indicates that a solid solution characterizes each assemblage [19,25,26] (Figure 4). The intermediate type between assemblages I and II was found in the fractured slag, which contains primary phases that are mainly dendritic willemite and fayalite that appear to have crystallized simultaneously. The crystallization temperatures of willemite and fayalite are similar, which suggests that the crystallization sequence of willemite and fayalite is controlled by the melt Zn/Fe ratio.

Spinel group phases found in the slag are magnetite and gahnite. Magnetite ($\text{Fe}^{2+}\text{Fe}^{3+}_2\text{O}_4$) is an isometric-hexoctahedral crystal that can contain Al and Zn. Magnetite appears to have crystallized from Fe-rich and Zn-poor melt in the slag. On average, skeletal magnetite crystals are slightly richer in Al than are euhedral crystals. Gahnite (ZnAl_2O_4) is an isometric crystal rarely found in assemblage I, coexisting with Zn-rich glass (Table 3).

Figure 4. Scattered diagrams of Zn/Fe rate (A) in willemite and fayalite (B) in fayalite disaggregated by the assemblages. AI: assemblage I; AII: assemblage II; AIII: assemblage III.

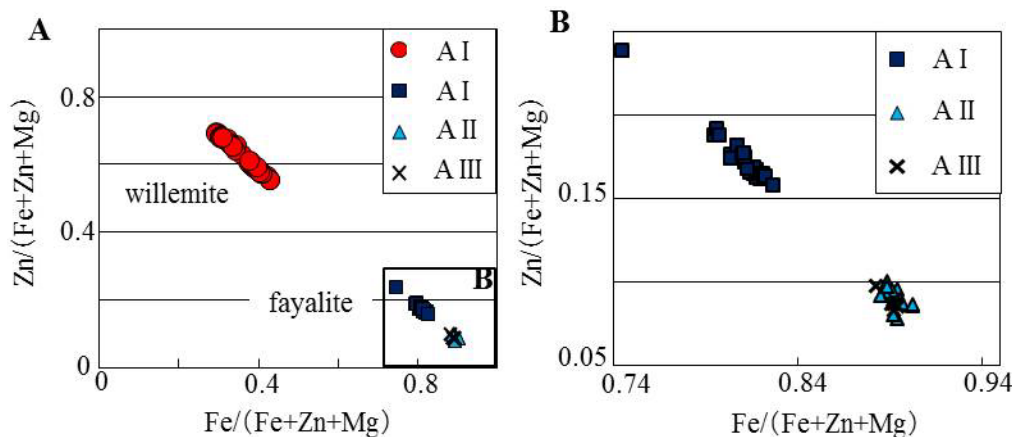


Table 3. Chemical compositions of spinel group phases obtained by EDS. “-” indicates non-detected. Structural formulae (apfu: atoms per formula unit) were calculated on the basis of four oxygens.

Phases	Magnetite		Gahnite	
Al ₂ O ₃ (wt %)	4.04	2.93	47.65	46.78
FeO (wt %)	87.70	87.19	22.88	24.63
ZnO (wt %)	3.74	5.68	31.18	30.31
MgO (wt %)	0.33	-	-	-
Total (wt %)	95.81	95.80	101.71	101.72
Al (apfu)	0.23	0.17	1.78	1.75
Fe ²⁺ (apfu)	3.50	0.35	0.61	0.66
Zn (apfu)	0.13	0.20	0.73	0.71
Mg (apfu)	0.02	-	-	-

3.2.3. Sulfides and Metallic Phases

Sulfides and metallic phases occur as matte drops that formed by liquid immiscibility from the matte component in the slag during smelting. Matte drops in assemblages I and II mainly comprise metallic Cu, Cu sulfides, and Cu-bearing alloys (Table 4). Matte drops in assemblage III are mainly composed of metallic Cu and Cu–Fe alloy. The matte drops also include partially formed, compounds containing Fe, Zn, S, As, Ag, and/or Sn with a wide range of chemical compositions.

In the massive slag, the abundance of matte drops is only *ca.* 10 vol %. However, the sulfides and metallic phases contain high concentrations of metals and could potentially release toxic metals into the environment during alteration and dissolution.

Table 4. Chemical compositions of matte drops obtained by EDS. “-” indicates non-detected. iss: intermediate solid solution.

Phases	Matte Drops								
	Assemblage I			Assemblage II			Assemblage III		
	Alloy	Sphalerite	Fe-Cu iss	Alloy	Fe-Cu iss	Fe-Cu iss	Alloy	Alloy	Fe-Cu iss
	<i>Cu-Sn-Fe-Ag</i>	<i>Zn_{7.4}Fe_{1.1}S₈</i>	<i>Cu_{7.5}Fe_{0.3}S₅</i>	<i>Cu-Fe-As-Sn</i>	<i>Fe_{0.6}Cu_{0.4}S</i>	<i>Cu_{1.2}Fe_{0.4}S</i>	<i>Cu-Fe</i>	<i>Cu-Fe-As-Sn</i>	<i>Cu_{0.9}Fe_{0.1}S</i>
S (wt %)	-	33.88	24.52	-	34.90	25.46	-	-	20.13
Fe ²⁺ (wt %)	1.00	7.95	2.28	3.53	35.68	16.17	2.84	2.30	3.19
Cu (wt %)	59.97	-	72.96	91.53	29.65	58.98	97.28	94.66	76.10
Zn (wt %)	-	57.74	-	-	-	-	-	-	-
As (wt %)	-	-	-	3.36	-	-	-	1.61	-
Ag (wt %)	0.79	-	-	-	-	-	-	-	-
Sn (wt %)	38.18	-	-	1.66	1.65	-	-	0.96	-
Total (wt %)	99.94	99.06	99.76	100.08	101.89	100.61	100.12	99.53	99.42
S (at %)	-	33.88	24.52	-	34.90	25.46	-	-	33.34
Fe ²⁺ (at %)	1.39	7.95	2.28	3.53	35.68	16.17	3.21	2.64	3.04
Cu (at %)	73.06	-	72.96	91.53	29.65	58.98	96.79	95.47	63.62
Zn (at %)	-	57.74	-	-	-	-	-	-	-
As (at %)	-	-	-	3.36	-	-	-	1.37	-
Ag (at %)	0.56	-	-	-	-	-	-	-	-
Sn (at %)	24.90	-	-	1.66	1.65	-	-	0.52	-

3.2.4. Glass

Glass in the slag is mainly composed of Si and Al, but also contains Fe and Zn (Table 5). The glassy matrix contains micro-dendritic/skeletal fayalite, Fe-rich micro-particles, and fine-grained matte drops (<1–3 μm). The slag also contains other types of Si-rich glassy materials derived from the unmelted gangue. The glassy materials locally contain quartz, albite, and anorthite. Although slag glass can react with water and atmospheric gases during weathering, in the present study it does not contain high concentrations of potentially toxic metals and metalloids compared with other crystalline and metallic phases.

3.3. Metal and Metalloid Concentrations in Slag

Assemblage I characteristically contains high concentrations of Zn. In contrast, assemblage III contains high concentrations of Fe and Cu (Table 6). Metal and metalloid concentrations, in particular Fe and Zn, are affected by compositional differences in the primary phases (Figure 5). Zn concentrations decrease from assemblage I to III, whereas Fe concentrations increase. Other elements show different distribution patterns to those of Zn and Fe. Assemblage III contains the highest concentrations of Cu, however, it is a rare assemblage at the study site. Assemblage I, the main assemblage at the study site, contains the highest total concentrations of potentially toxic elements, and therefore, has the highest potential for toxic pollution.

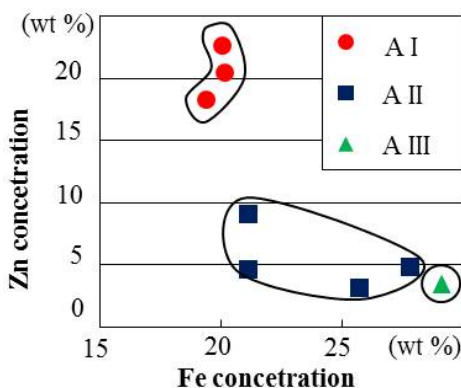
Table 5. Chemical compositions of glass obtained by EDS. Matrix: glass in matrix; Others: Si-rich glassy materials. “-” indicates non-detected.

Assemblages (wt %)	Assemblage I				Assemblage II		Assemblage III			
	Matrix		Others		Matrix		Matrix		Others	
SiO ₂	56.84	50.43	93.21	98.99	48.20	52.03	51.51	61.76	66.35	57.64
Al ₂ O ₃	10.89	16.83	3.38	0.23	16.97	20.00	16.67	8.46	21.63	32.11
Na ₂ O	0.70	1.19	0.24	-	0.91	1.21	1.08	0.99	0.66	0.44
CaO	6.94	0.67	-	-	0.53	0.84	2.43	1.27	-	-
MgO	-	-	0.22	-	-	-	-	-	0.40	-
K ₂ O	0.99	1.09	0.58	-	1.30	1.12	2.29	2.19	3.51	2.08
FeO	15.23	17.44	2.31	0.75	24.14	15.37	21.50	13.58	3.41	4.09
TiO ₂	-	0.57	-	-	0.56	0.38	-	-	0.22	-
ZnO	6.53	11.75	-	-	7.79	9.39	4.50	2.47	-	-
CuO	-	-	-	-	-	-	-	9.10	1.16	0.62
SnO	1.42	-	-	-	-	-	-	-	-	-
Total	99.54	99.97	99.93	99.93	100.40	100.34	99.98	99.82	98.22	96.98

Table 6. Metal and metalloid concentrations of slag obtained by ED-XRF. “-” indicates non-detected.

Assemblages	Assemblage I			Assemblage II				Assemblage III
Fe (wt %)	20.2	19.4	20.1	27.8	21.2	25.7	21.2	29.2
Zn (wt %)	20.4	18.3	22.7	4.83	4.68	3.21	9.13	3.43
Cu (ppm)	10,600	6,880	10,400	7,110	7,890	6,760	11,500	16,300
As (ppm)	582	-	-	391	377	119	-	421
Cd (ppm)	-	-	-	-	-	-	116	-
Sn (ppm)	1,840	869	1,040	3,450	1,530	1,140	1,790	3,100
Pb (ppm)	761	374	209	-	84.8	142	826	-

Figure 5. A scattered diagram of Zn/Fe concentrations in each assemblage. AI: assemblage I; AII: assemblage II; AIII: assemblage III.



3.4. Natural Weathering Features of Slag

A massive component of the slag contains particularly high concentrations of toxic metals, S, and As, largely present in willemite and/or matte drops. Weathering of the massive component in

assemblage I could have an important impact on pollution at this site and, as such, this study focuses on the natural weathering features of assemblage I.

The weathered zone within the slag was indicated by the presence of weathered willemite. The quantitative maps indicate that Si, S, Cu, and Zn concentrations in the weathered zone are lower than in the unweathered zone (Figure 6). In contrast, Fe concentrations are almost the same in both zones. The unweathered zone is mainly composed of euhedral willemite and the matrix is largely dendritic fayalite. Silicate glass and matte drops are present in the matrix. Fayalite was identified in the matrix of the weathered zone by both EDS and XRD. However, willemite was identified as a minor component, or was absent from the weathered zone. These results indicate that willemite and matte drops are being altered to other crystalline phases or amorphous materials.

The outer edges of willemite in the weakly weathered zone have been altered to Zn-bearing iddingsite-like phases and/or Fe-hydroxides (Figure 7a). The weathered edges of willemite gradually change from an iddingsite-like phase to Fe-hydroxides during progressive weathering. Pseudomorphs of willemite in the strongly weathered zone are mainly composed of Fe-hydroxides (Figure 7b). Zn concentration in willemite decreases with progressive weathering (Figure 8). The Fe-hydroxides contain lower Zn and higher Fe concentrations as compared with primary willemite (Table 7). In contrast, the fayalite-bearing matrix is almost never altered in the strongly weathered zone. Willemite contains Zn in four-fold coordination, whereas fayalite contains Fe in six-fold coordination [27]. Therefore, the binding strength of Fe in fayalite is greater than that of Zn in willemite. Zn coordination in willemite changes during conversion to its hydrated aqueous phase, which facilitates relatively rapid and easier dissolution of Zn from willemite [27].

In the weathered zone, matte drops weather along cracks and at their rims, and are converted to Fe-hydroxides as well as willemite (Figure 7c). The Fe concentrations of areas adjacent of cracks and rims increase relative to unweathered matte drops. Metal and/or S concentrations in matte drops decrease with progressive weathering (Figure 8).

Figure 6. A back-scattered electron image and quantitative elemental maps of unweathered/weathered massive component of slag obtained by SEM-EDS. Fa: fayalite; Wi: willemite; MD: matte drop.

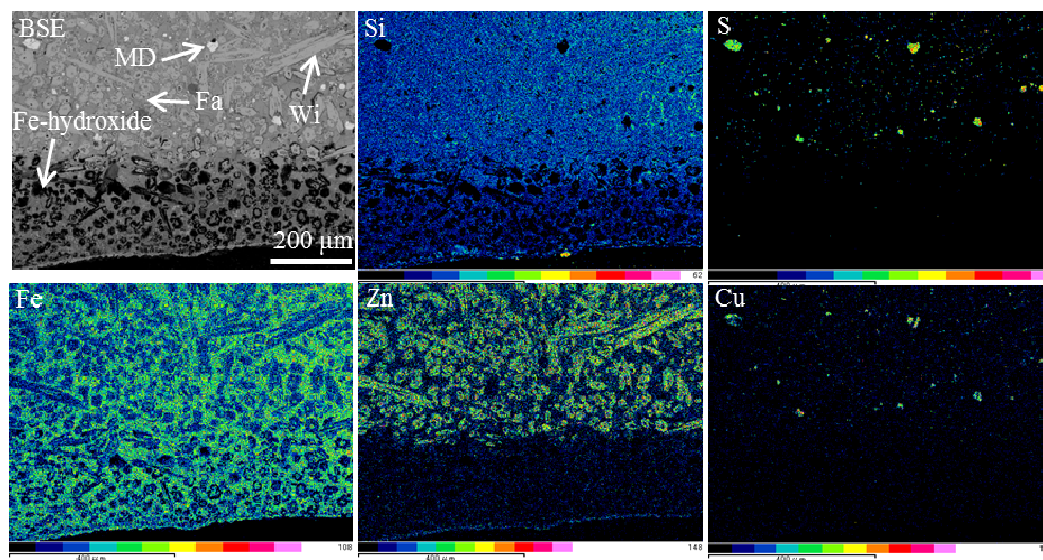


Figure 7. Back-scattered electron images of (a) a weakly weathered matte drop and willemite with iddingsite-like phases; (b) pseudomorphs of willemite in strongly weathered zone; and (c) a pseudomorph of matte drop in strongly weathered zone. Fa: fayalite; Wi: willemite; MD: matte drop; Id: iddingsite.

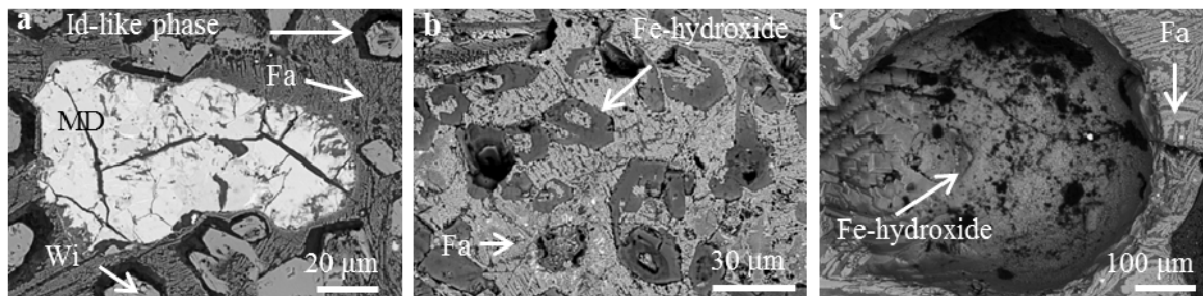
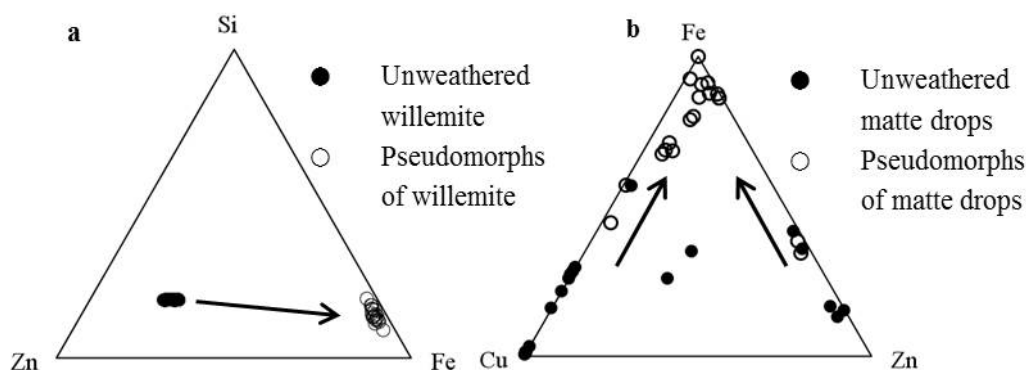


Table 7. Chemical compositions of pseudomorphs of willemite and matte drop obtained by EDS. Wi: willemite; MD: matte drop. “-” indicates non-detected.

Phases (wt %)	Pseudomorphs of Wi			Pseudomorphs of MD		
S	-	-	0.38	1.05	2.01	6.35
Al	2.05	1.94	2.53	-	-	-
Si	8.94	7.92	5.93	7.99	5.05	3.65
Ca	0.49	-	0.5	-	-	-
Fe	36.59	37.3	36.57	39.19	37.93	38.85
Cu	2.32	2.40	3.02	0.38	12.08	13.14
Zn	1.41	1.25	1.57	6.03	3.28	4.85
As	2.35	2.96	5.13	-	-	-
Sn	-	-	-	-	1.43	-
Total	79.86	79.20	80.29	54.63	61.78	66.84

Figure 8. Ternary diagrams of (a) Si-Zn-Fe concentrations of unweathered and pseudomorphs of willemite and (b) Fe-Cu-Zn concentrations of unweathered and pseudomorphs of matte drops.



Silicate glass in the slag at the study site contains predominantly Si, Fe, and Al; relatively little of the glassy phase is present compared with other phases. The thickness of one massive slag in this study is *ca.* 10 cm. The quenched glassy slag margin makes up several percent of the massive slag, and the total glass makes up <30 vol % of the massive slag. These results highlight that weathering of the

massive slag, which contains large amounts of willemite and matte drops, is the dominant contributor to potentially toxic element pollution of the surrounding environment. Stream water at the study site contains metal and metalloid abundances in the order $Zn \gg Fe > Cu > As > Pb$ (Table 8). Neutral-pH fluids promote precipitation of Cu-bearing phases but selectively mobilize Zn to some extent [14]. Therefore, weathering of willemite in the slag on the mine dump is a potential source of the Zn pollution in local stream water.

Table 8. Maximum potentially toxic elemental concentrations of stream water and sediments in a waste dump in Okayama, Japan and pollution standard values (PSV) stipulated by the ministry of health, labor, and welfare and the ministry of the environment in Japan. (1000) in PSV for Zn and Cu indicates a toxicity levels for aquatic habitats. DW: dry weight [21].

Elements	Zn	Cu	As	Pb
Stream water ($\mu\text{g/L}$)	1910	157	43.1	0.29
PSV ($\mu\text{g/L}$)	(1000)	(1000)	10	10
Sediment (mg/kg-DW)	3800	6240	4630	286
PSV (mg/kg-DW)	-	-	150	150

4. Conclusions

The slag examined in this study contains high concentrations of Zn and Cu and also includes other potentially toxic elements such as As and Cd. The slag is mainly composed of assemblage I, containing large concentrations of potentially toxic elements stored in willemite and matte drops that are susceptible to weathering. The matte drops contain variable amounts of S, Fe, Zn, As, Ag, and/or Sn in addition to Cu. Willemite alters more rapidly than the other phases in slag and is converted to Fe-hydroxide. Zn is dissolved during the weathering of willemite. Other heavy metals and As are dissolved by weathering of the matte drops. The slag also contains Cd that has a high potential for toxicity. Therefore, weathering of the artisanal metallurgical slag may be a major contributor to pollution of the surrounding environment.

Acknowledgments

The authors are grateful to Dr. H. Ohfuji (Ehime University, Japan) for help with analysis by SEM-EDS. We thank Ms. H. Akamatsu (Ehime University, Japan) for help with making thin sections. We thank the three anonymous referees for their perceptive comments and recommendations. This study was partially supported by grant from Fukada Geological Institute (Fukada Grant-in-Aid, 2013).

Conflicts of Interest

The authors declare no conflict of interest.

References

1. Costagliola, P.; Benvenuti, M.; Chiarantini, L.; Bianchi, S.; Benedetto, F.D.; Paolieri, M.; Rossato, L. Impact of ancient metal smelting on arsenic pollution in the Pecora River Valley, Southern Tuscany, Italy. *Appl. Geochem.* **2008**, *23*, 1241–1259.
2. Georgakopoulou, M.; Bassiakos, Y.; Philanitou, O. Seriphos surface: A study of Cu slag heaps and Cu sources in the context of Early Bronze Age Aegean metal production. *Archaeometry* **2010**, *53*, 123–145.
3. Sáez, R.; Nocete, F.; Nieto, J.M.; Capitán, M.Á.; Rovira, S. The extractive metallurgy of copper from Cabezo Juré, Huelva, Spain: Chemical and mineralogical study of slags dated to the third millennium B.C. *Can. Mineral.* **2003**, *41*, 627–638.
4. Manz, M.; Castro, L.J. The environmental hazard caused by smelter slags from the Sta. Maria de la Paz mining district in Mexico. *Environ. Pollut.* **1997**, *98*, 7–13.
5. Teng, Y.; Tuo, X.; Ni, S.; Zhang, C.; Xu, Z. Environmental geochemistry of heavy metal concentrations in soil and stream sediment in Panzhihua mining and smelting area, Southwestern China. *Chin. J. Geochem.* **2003**, *22*, 253–262.
6. Wilson, N.J.; Craw, D.; Hunter, K. Antimony distribution and environmental mobility at an historic antimony smelter site, New Zealand. *Environ. Pollut.* **2004**, *129*, 257–266.
7. Vdović, N.; Billon, G.; Gabelle, C.; Potdevin, J.L. Remobilization of metals from slag and polluted sediments (Case study: The canal of the Deûle river, northern France). *Environ. Pollut.* **2006**, *141*, 359–369.
8. Douay, F.; Pruvot, C.; Roussel, H.; Ciesielski, H.; Fourier, H.; Proix, N.; Waterlot, C. Contamination of urban soils in an area of northern France polluted by dust emission of two smelters. *Water Air Soil Pollut.* **2008**, *188*, 247–260.
9. Piatak, N.M.; Seal, R.R., II; Hammarstrom, J.M. Mineralogical and geochemical controls on the release of trace elements from slag produced by base- and precious-metal smelting at abandoned mine site. *Appl. Geochem.* **2004**, *19*, 1039–1064.
10. Navarro, A.; Cardellach, E.; Mendoza, J.L.; Corbella, M.; Domènech, L.M. Metal mobilization from base-metal smelting slag dumps in Sierra Almagrera (Almería, Spain). *Appl. Geochem.* **2008**, *23*, 895–913.
11. Vítková, M.; Ettler, V.; Johan, Z.; Kříbek, B.; Šebek, O.; Mihaljevič, M. Primary and secondary phases in copper-cobalt smelting slags from the Copperbelt Province, Zambia. *Mineral. Mag.* **2010**, *74*, 581–600.
12. Ettler, V.; Johan, Z.; Kříbek, B.; Šebek, O.; Mihaljevič, M. Mineralogy and environmental stability of slags from the Tsumeb smelter, Namibia. *Appl. Geochem.* **2009**, *24*, 1–15.
13. Gee, C.; Ramsey, M.H.; Maskall, J.; Thornton, I. Mineralogy and weathering process in historical smelting slags and their effect on the mobilisation of lead. *J. Geochem. Explor.* **1997**, *58*, 249–257.
14. Lottermoser, B.G. Mobilization of heavy metals from historical smelting slag dumps, north Queensland, Australia. *Mineral. Mag.* **2002**, *66*, 475–490.

15. Ettler, V.; Legendre, O.; Bodéan, F.; Touray, J.C. Primary phases and natural weathering of old lead-zinc pyrometallurgical slag from Příbram, Czech Republic. *Can. Mineral.* **2001**, *39*, 873–888.
16. Collins, R.J.; Miller, R.H. Utilization of mining and mineral processing wastes in the United States. *Mineral. Environ.* **1979**, *1*, 8–19.
17. Piatak, N.M.; Seal, R.R., II. Mineralogy and the release of trace elements from slag from the Hegeler Zinc smelter, Illinois (USA). *Appl. Geochem.* **2010**, *25*, 302–320.
18. Shanmuganathan, P.; Lakshmipathiraj, P.; Srikanth, S.; Nachiappan, A.L.; Sumathy, A. Toxicity characterization and long-term stability studies on copper slag from the ISASMRLT process. *Resour. Conserv. Recycl.* **2008**, *52*, 601–611.
19. Raghavan, V. Fe-O-Si-Zn (Iron-Oxygen-Silicon-Zinc) *J. Phase Equilibria Diffus.* **2000**, *31*, 385–386.
20. Nishizono, H.; Ichikawa, H.; Suzuki, S.; Ishii, F. The role of the root cell wall in the heavy metal tolerance of *Athyrium yokoscense*. *Plant Soil* **1987**, *101*, 15–20.
21. Sakakibara, M.; Ohmori, Y.; Ha, N.T.H.; Sano, S.; Sera, K. Phytoremediation of heavy metal-contaminated water and sediment by *Eleocharis acicularis*. *Clean-Soil Air Water* **2011**, *39*, 735–741.
22. Imai, N.; Terashima, S.; Itoh, S.; Ando, A. 1996 Compilation of analytical data on nine GSJ geochemical reference samples, “Sedimentary Rock Series”. *Geostand. Newsl.* **1996**, *20*, 165–216.
23. Imai, N.; Terashima, S.; Itoh, S.; Ando, A. 1998 Compilation of analytical data for five GSJ geochemical reference samples: The “Instrumental Analysis Series”. *Geostand. Newsl.* **1999**, *23*, 223–250.
24. Parsons, M.B.; Bird, D.K.; Einaudi, M.T.; Alpers, C.N. Geological and mineralogical controls on trace element release from the Penn Mine base-metal slag dump, California. *Appl. Geochem.* **2001**, *16*, 1567–1593.
25. Jak, E.; Zhao, B.; Hayes, P.C. Experimental study of phase equilibria in the systems Fe-Zn-O and Fe-Zn-Si-O at metallic iron saturation. *Metall. Mater. Trans. B* **2000**, *31*, 1195–1201.
26. Jak, E.; Degterov, S.; Pelton, A.D.; Hayes, P.C. Coupled experimental and thermodynamics study of the Zn-Fe-Si-O system. *Metall. Mater. Trans. B* **2001**, *32*, 793–800.
27. Velbel, M.A. Bond strength and the relative weathering rates of simple orthosilicates. *Am. J. Sci.* **1999**, *299*, 679–696.